







Intertwining of lasing and superradiance under spintronic pumping

Oksana Chelpanova ¹, Alessio Lerose ², Shu Zhang ^{3,4}, Iacopo Carusotto ⁵,
Yaroslav Tserkovnyak ⁴ and Jamir Marino ^{1,6}

¹*Institut für Physik, Johannes Gutenberg Universität Mainz, D-55099 Mainz, Germany*

²*Department of Theoretical Physics, University of Geneva, Quai Ernest-Ansermet 30, 1205 Geneva, Switzerland*

³*Max-Planck-Institut für Physik komplexer Systeme, 01187 Dresden, Germany*

⁴*Department of Physics and Astronomy and Bhaumik Institute for Theoretical Physics,
University of California, Los Angeles, California 90095, USA*

⁵*INO-CNR BEC Center and Dipartimento di Fisica, Università di Trento, 38123 Trento, Italy*

⁶*Kavli Institute for Theoretical Physics, University of California, Santa Barbara, California 93106, USA*



(Received 22 December 2021; revised 12 April 2022; accepted 26 July 2023; published 5 September 2023)

We introduce a quantum optics platform featuring the minimal ingredients for the description of a spintronically pumped magnon condensate, which we use to promote driven-dissipative phase transitions in the context of spintronics. We consider a Dicke model weakly coupled to an out-of-equilibrium bath with a tunable spin accumulation. The latter is pumped incoherently in a fashion reminiscent of experiments with magnet-metal heterostructures. The core of our analysis is the emergence of a hybrid lasing-superradiant regime that does not take place in an ordinary pumped Dicke spin ensemble, and which can be traced back to the spintronics pumping scheme. We interpret the resulting nonequilibrium phase diagram from both a quantum optics and a spintronics standpoint, supplying a conceptual bridge between the two fields. The outreach of our results concern dynamical control in magnon condensates and frequency-dependent gain media in quantum optics.

DOI: [10.1103/PhysRevB.108.104302](https://doi.org/10.1103/PhysRevB.108.104302)

I. INTRODUCTION

The theme of dynamical phase transitions enabled by the interplay of interactions, drive, and dissipation permeates different branches of quantum many-body physics, such as quantum optics [1,2], cold atoms [3,4], and nonequilibrium solid-state physics [5–7]. The interest in them ranges from practical applications in dynamical control to the fundamentals of statistical mechanics. The exploration and understanding of nonequilibrium phases would benefit from a unifying language, which, however, remains elusive due to the diversity of microscopic ingredients, relevant scales, and engineering capabilities across the various platforms.

In this paper, we take the first step in filling this gap by studying a bare-bones model that offers complementary interpretations pertinent to both spintronics and driven-dissipative quantum optics, as illustrated in Fig. 1(a). The model is inspired by typical considerations in spintronics and cavity quantum electrodynamics (QED) systems and contains the ingredients that can be implemented in both platforms. We construct the model by coupling a coherent subsystem to an incoherent one through weak $U(1)$ symmetric interactions—the former is a Dicke model featuring a \mathbb{Z}_2 symmetric interaction between a spin ensemble and a boson mode, while the latter is a spin ensemble that can be externally driven into a given population state. The coherent subsystem is thus indirectly pumped.

As we will show, the interplay between the spin pumping and the Dicke coupling opens a parameter space where the lasing phase, which corresponds to the breaking of $U(1)$ symmetry, and the superradiant (SR) phase, which corresponds to breaking of \mathbb{Z}_2 symmetry, intertwine and lead to dynamical regimes exhibiting features of both. From the spintronics

point of view, this implies the possibility of magnon lasing in a system with strongly broken $U(1)$ symmetry. From the quantum optics perspective, the model proposes an indirect pumping scheme which can lead to unconventional dynamical phases. In particular, a dynamical phase emerges with intertwined lasing and superradiance features, which results from a pumping scheme inspired by spintronics while also realizable in a quantum many-body optics platform. We argue that the nontrivial implications of our model in both fields can provide a conceptual bridge between the two communities.

A. Structure of the paper

The paper is organized as follows. First, we motivate this study from the separate cavity QED and spintronics backgrounds. We highlight the additional ingredients and briefly examine their effects on the conventionally expected dynamics in both setups. In Sec. II, we discuss the minimal model that captures these ingredients and draw parallels between implementations in the two setups. We also discuss the known limits of the resulting model. In Sec. III, we solve the dynamics of the model in the mean-field approximation and discuss the dynamical phase diagram, remarking on the symmetry breaking in different dynamical phases of the model. Finally, in Sec. IV we discuss the mechanism to generate unique dynamical phases and how they can be controlled via external drive. We conclude in Sec. V by discussing further developments of the model in light of recent advancements in the control of the cavity QED and spintronics platforms.

B. Cavity QED background and context

Cavity QED is a field of study that focuses on the interaction between light and matter at the quantum level. Over

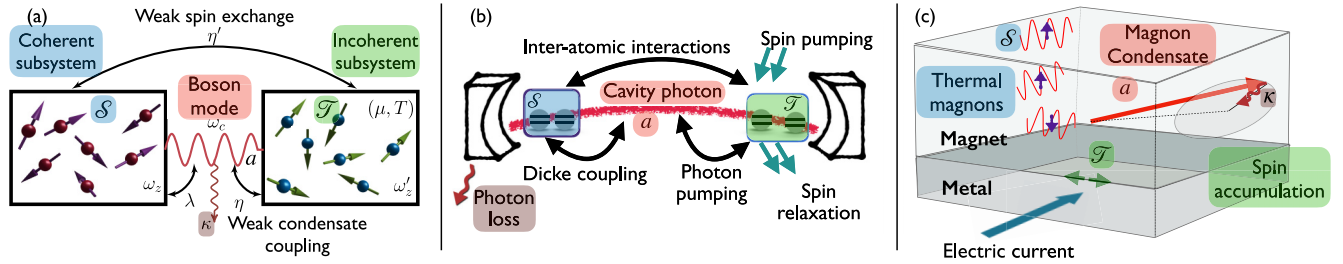


FIG. 1. (a) An ensemble of spins-1/2 S (in blue) is coupled to a boson mode (in red) which models a magnon condensate or a cavity boson which can become macroscopically occupied for large values of the Dicke coupling, λ . It is also coupled to a spin-1/2 subsystem T (in green) under incoherent spin relaxation and pumping controlled by the spin accumulation μ and temperature T . The population inversion of T can induce a coherent dynamical response in S , which is the central mechanism explored in this paper. Dissipation with strength κ (in brown) acts on the boson mode and is shown by a red wiggly line. The model contains the essential ingredients of both quantum optics (b) and spintronics (c) platforms, as detailed in the main text. Corresponding elements in different setups are highlighted in the same color.

the years, multiple platforms have been proposed and realized as quantum simulators for exploring exotic models and developing desired phases of matter [8–11]. Specifically, by combining multiple driving fields, few cavity modes, and separating particles in a cavity via tweezers, exotic spin-spin interactions can be realized in cavity QED experiments [10,12] as well as nonlocal dissipation that leads to more efficient control over quantum correlations [13–15]. Furthermore, different experiments have varying system sizes, ranging from a few atoms per cavity, which require a complete quantum mechanical treatment, to hundreds of thousands of particles per cavity, which can be treated classically [16–18]. All these factors make cavity QED setups highly flexible and promising candidates for realizing various driven-dissipative models.

In this paper, we introduce a schematic model that well captures the dynamical features of the setup depicted in Fig. 1(b). We consider an optical cavity where two species of two-level atoms, S and T , are coupled to each other as well as to a common lossy cavity mode. The ensemble S collectively couples to the cavity photon via a \mathbb{Z}_2 symmetric term as in the Dicke model, while the ensemble T is incoherently pumped and couples to the same photon mode via a spin-boson interaction $U(1)$ symmetric term as in a Tavis-Cummings model. Combining these two models together brings us to the dynamical phase which hybridly inherits properties of both stationary and nonstationary phases.

Experimentally engineering photon-matter interaction with one spin species and one cavity mode is nowadays at its state of the art [9]. While combining two spin species may be challenging, the first steps have been taken, such as considering multicomponent BECs in a cavity [19–21] or building an effective spin representation based on different degrees of freedom, for example, momentum spin states and internal spin states [22,23].

C. Spintronics background and context

Our motivation to separate the coherent (S) and incoherent (T) spin subsystems stems from a solid-state viewpoint, to allow quantum correlations to settle in without much disruption from direct pumping processes. Considering magnet-metal heterostructures [24–32] as a primary example, the magnet

layer has a stiff order parameter accompanied by coherent excitations [33], while itinerant electrons carrying incoherent spins in the metal layer are more amenable to external control [34]. One of the consequences of the magnet being a strongly interacting system is the propensity of a long-wavelength magnon to undergo (Bose-Einstein) condensation [35–37], which is mimicked by the boson mode in our model. In a magnet, such condensation can manifest as a static phase transition [38] or a dynamical one with the magnetic order parameter precessing spontaneously [39–41], bearing analogy to the SR and lasing transitions, respectively. As shown in Fig. 1(c), a magnon condensation can be triggered by electrically pumping the heterostructure [42–46]. A spin accumulation is induced via the spin Hall effect in the metal [47–52] and exerts a spin torque [53–55] on the magnetic dynamics by interfacial magnon-electron scatterings. Such a torque can overcome the intrinsic magnon decay and maintain a quasiequilibrium condensate of magnons. In addition, the magnon condensate and the thermally occupied short-wavelength magnons undergo coupled dynamics, previously described by a two-fluid theory [56]. Our model, though much simplified from this practical scenario, allows for a full treatment of the interplay of spin pumping, coupling between the interacting magnetic excitations and the pumped reservoir, and dissipative effects.

We remark that the model considered in this paper should not be regarded as an *ab initio* description of the spintronic setup depicted in Fig. 1(c), rather it captures the key conceptual elements, especially from a symmetry point of view. To give more details, the interactions between long-wavelength a and short-wavelength S magnons in magnets are likely to involve higher-order terms in the spin operators, while here it is set to be a \mathbb{Z}_2 symmetric interaction, which can be an oversimplification. On the other hand, from the symmetries point of view, \mathbb{Z}_2 -type of $U(1)$ breaking commonly exists in magnetic materials, for example, due to crystalline anisotropy, and a Dicke term gives the desired symmetry. This induces ellipticity in magnon lasing, where the spontaneous precession of the magnon condensate is non-circular due to an oscillating magnitude. As we will show, an interesting form of magnon lasing, more dramatic than ellipticity, may arise when the $U(1)$ breaking term is sufficiently strong.

II. MODEL

The minimal model that captures the cavity QED setup in Fig. 1(b) and metal-magnet heterostructure in Fig. 1(c) is given in Fig. 1(a). Here we consider a Dicke sample [57–61], which consists of an ensemble \mathcal{S} of N spin-1/2's collectively coupled to a boson mode a of frequency ω_c , weakly interacting with an ensemble \mathcal{T} of an additional set of N spins. The level splitting of spins in subsystem \mathcal{S} (\mathcal{T}) is ω_z (ω'_z). The full Hamiltonian reads

$$H = \omega_c a^\dagger a + \omega_z \mathcal{S}^z + \omega'_z \mathcal{T}^z + \frac{\lambda}{\sqrt{N}} (a + a^\dagger) (\mathcal{S}^+ + \mathcal{S}^-) + \frac{\eta}{\sqrt{N}} (a \mathcal{T}^+ + a^\dagger \mathcal{T}^-) + \frac{\eta'}{N} (\mathcal{S}^+ \mathcal{T}^- + \mathcal{S}^- \mathcal{T}^+), \quad (1)$$

where a and a^\dagger are boson annihilation and creation operators mimicking the magnon condensate or the cavity photon, while the collective spin operators $\mathcal{S}^- = \sum_{i=1}^N \sigma_i^-$ and $\mathcal{T}^- = \sum_{i=1}^N \tau_i^-$ describe two various spin species in a cavity QED setup or thermal magnons and spins of conducting electrons in magnet-metal heterostructure. Here σ_i^α and τ_i^α with $\alpha = x, y, z$ are spin-1/2 operators and $\sigma^\pm = (\sigma^x \pm i\sigma^y)$. Here, we have introduced the Dicke coupling λ , a small boson-spin interconversion term η , and a small spin exchange coupling η' , the latter two quantifying the strength of $U(1)$ symmetric interactions between the spin ensemble \mathcal{T} with the boson mode a and spin ensemble \mathcal{S} , respectively. All couplings are normalized such that every term in the Hamiltonian Eq. (1) scales linearly with the system size N .

The pumping and dissipative effects are described by the following Lindblad master equation [62] for the joint density matrix of the total system:

$$\frac{d\rho}{dt} = -i[H, \rho] + \kappa \mathcal{D}[a] + \gamma_\uparrow \sum_{i=1}^N \mathcal{D}[\tau_i^+] + \gamma_\downarrow \sum_{i=1}^N \mathcal{D}[\tau_i^-]. \quad (2)$$

Here, the dissipators $\mathcal{D}[x] \equiv x\rho x^\dagger - 1/2\{x^\dagger x, \rho\}$ are defined as usual. The ensemble \mathcal{T} is driven incoherently and, in the steady state of the Lindblad, reaches a grand canonical state parameterized by temperature T and spin accumulation μ as a result of the spin pump and loss rates $\gamma_\uparrow = \gamma_t/[1 + e^{\beta(\omega'_z - \mu)}]$ and $\gamma_\downarrow = \gamma_t/[1 + e^{-\beta(\omega'_z - \mu)}]$, where $\beta = T^{-1} > 0$ and $\gamma_t = \gamma_\uparrow + \gamma_\downarrow \geq 0$. In Eq. (2), we have neglected spin dephasing effects [57]. In cavity QED, the Lindbladian (2) models spin pumping, used to induce the lasing phase [60,63], while in spintronics it mimics the fact that the spin accumulation between metal and magnet layers in Fig. 1(c) results from the spin Hall effect and, thus, can be controlled by changing the current in the metal layer [47–52]. When $\mu > \omega'_z$, the incoherent subsystem \mathcal{T} experiences a population inversion which can be transferred to the rest of the system via η and η' and triggers a lasing instability.

In the dissipative dynamics of Eq. (2), we have also considered photon loss with rate κ to model finite linewidth of the cavity photon. The relaxation of the collective bosonic mode in a magnet, on the other hand, depends self-consistently on its dynamics [64]. We therefore consider, as an alternative, a viscous damping of the magnon condensate whenever the

direct applications to spintronics are pertinent. In terms of magnetic dynamics, the phenomenological Gilbert damping [65] slows down the coherent precession of the order parameter and brings it towards the global equilibrium state [54,66]. Interestingly, our results remain qualitatively unaltered under dissipation through photon loss or Gilbert damping, see Appendix C.

Since our model (1) describes collective all-to-all interaction between spins, all quantum effects come from the noncommutativity of collective spins [$S^\alpha/N, S^\beta/N = i\epsilon_{\alpha\beta\gamma} S^\gamma/N^2 \propto 1/N$, which sets the effective Planck's constant of the model $\hbar_{\text{eff}} \propto 1/N$ [67,68], (identical commutation relations hold for \mathcal{T} spins). Thus, in the thermodynamic limit, $N \rightarrow \infty$, the mean-field treatment becomes exact [59,69,70]. From now on, we use the normalized variables $a \propto a/\sqrt{N}$, $\mathcal{S} \propto \mathcal{S}/N$, $\mathcal{T} \propto \mathcal{T}/N$, as is customary in the treatment of systems with collective light-matter interactions [57–59]. See Appendix A for the mean-field equations of motion of the normalized variables.

We start analyzing the model by revisiting some established dynamical regimes of the Hamiltonian in Eq. (1). The detailed solutions in the following two limits are discussed in Appendix B.

A. Dicke model

For $\eta = \eta' = 0$, we recover the Dicke model [59,71], which models photon-matter interaction in cavity QED. This model has been studied extensively theoretically [58,60,71,72] and implemented in few experimental platforms [18,73,74]. In the $N \rightarrow \infty$ limit, the Dicke model describes a second-order phase transition from the normal state (NS), in which $\langle \mathcal{S}^z \rangle = \pm 1/2$ and $\langle a^\dagger a \rangle = 0$ to a SR phase, which is associated with the spontaneous breaking of \mathbb{Z}_2 symmetry of the Hamiltonian and corresponds to $\langle \mathcal{S}^x \rangle \neq 0$ and $\langle a^\dagger a \rangle \neq 0$. Here $\langle \cdot \rangle$ stands for the ensemble-averaged value of an observable. This picture remains qualitatively valid when small couplings η and η' are switched on while the spin pumping is weak, namely, $\gamma_\uparrow < \gamma_t/2$ [cf. Fig. 2(a)].

B. Tavis-Cummings model

The limit $\eta' = \lambda = 0$ corresponds to the incoherently pumped Tavis-Cummings model [57,59,63,75–77]. The system in this case is endowed with a $U(1)$ symmetry, corresponding to conservation of the total number of excitations of the spins and the boson.

For $\gamma_t \gg \eta, \eta'$, the system quickly relaxes towards a steady state with $\langle \mathcal{T}^z \rangle \approx (\gamma_\uparrow - \gamma_\downarrow)/(2\gamma_t) \equiv \tau_0^z$ and $\langle \mathcal{T}^\pm \rangle \approx 0$. For $\gamma_\uparrow/\gamma_t \geq 1/2 + \kappa\gamma_t/(8\eta^2) + \kappa\gamma_t(\omega_c - \omega'_z)^2/(2\eta^2(\kappa + \gamma_t)^2)$, the nontrivial solution arises, where the symmetry is dynamically broken with $\langle a \rangle$ and $\langle \mathcal{T}^{x,y} \rangle$ undergoing oscillations. At long times, both $\langle \mathcal{T}^z \rangle$ and the photon number n approach the steady values set by the pumping rates $\gamma_{\uparrow/\downarrow}$; see Appendix B for more details. To acquire some intuitive insights, we take a look at the $\omega_c \approx \omega'_z \equiv \omega$ limit. In this case, the lasing solution is only possible when the photon loss rate is below a critical value, $\kappa < \kappa_c = 4\eta^2/\gamma_t$. In other words, given a finite photon loss rate, the lasing will be suppressed in the fast-relaxing ($\gamma_t \rightarrow \infty$) limit.

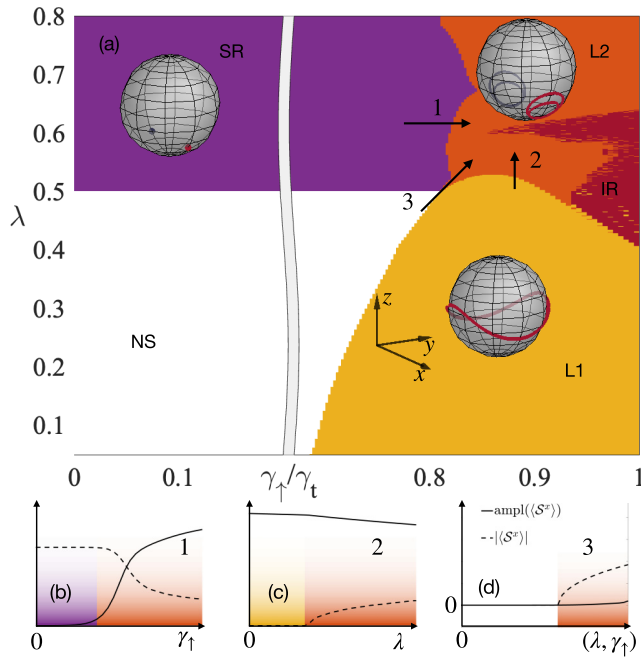


FIG. 2. Dynamical phases resulting from the interplay of spin pumping and Dicke coupling. (a) For $\gamma_\uparrow < \gamma_\downarrow/2$, the usual critical coupling ($\lambda_c \simeq 0.5$) associated to the Dicke transition separates the normal (NS) from the superradiant (SR) phase. For $\gamma_\uparrow > \gamma_\downarrow/2$, the normal state becomes unstable, and observables in the ensemble \mathcal{S} oscillate with zero average value of S^x in region L1, and around one of the minima of the SR phase in region L2, as shown in the Bloch spheres. Inside the irregular (IR) region the motion of the collective spin covers uniformly a large part of the Bloch sphere without any structured pattern and is suggestive of chaotic behavior. (b)–(d) The absolute value of time-averaged $\langle S^x \rangle$ (dashed line) and amplitude of its oscillations (solid line) along transition lines 1–3 in the main inset (a). Here we have chosen $\omega_c = \omega_z = \omega'_z = 1$, $\gamma_\downarrow = 1$, $\eta = \eta' = 0.1$, $\kappa = 0.06$.

III. DYNAMICAL PHASE DIAGRAM

By turning on the Dicke coupling λ together with sizable spin pumping in the weakly coupling limit ($\eta, \eta' \rightarrow 0^+$), we generate the diagram of dynamical responses [cf. Fig. 2(a)] in mean-field treatment. In Appendix A, we present the associated equations of motion; we also analyze the breakdown of the mean field from finite N corrections in Appendix E.

For strong pumping ($\gamma_\uparrow > \gamma_\downarrow/2$), the spins in the ensemble \mathcal{S} display long-lived oscillatory dynamics [see trajectories on the Bloch sphere in Fig. 2(a)]. Region L1 in Fig. 2(a) resembles the regular lasing [63] discussed above, while L2 features SR oscillations. The transition from L1 to L2 occurs around values of the Dicke coupling $\sim \lambda_c$, with a nonvanishing time average of $\langle S^x \rangle$ in L2. In this phase, we observe persistent oscillatory dynamics reminiscent of lasing around one of the symmetry-broken states of the Dicke model. Such SR oscillations would not arise by direct pumping the Dicke model through the Lindblad channels in Eq. (2) but rather a result of the pumping scheme in Fig. 1 inspired by spintronic scenarios. In return, the emergence of this dynamical phase is also implicative for further possibilities of dynamical phenomena in spintronics. In this regard, the dynamical phase

L2 is a conceptual bridge between the quantum optics and spintronics communities which we are aiming to lay out in this work. Notice that despite the pumped subsystem experiencing population inversion, the spin ensemble \mathcal{S} remains in a state with negative $\langle S^z \rangle$ in both phases L1 and L2.

We now discuss the role of symmetries in the oscillatory dynamics displayed in L1 and L2, and in the transitions between these two different regimes. For $\lambda = 0$, the photon number n does not oscillate. A nonzero value of λ breaks the $U(1)$ symmetry and oscillations in n can be attributed to ellipticity [78] in the spontaneous precession in the absence of S^z conservation. In fact, the dynamics are instead governed by a \mathbb{Z}_2 symmetry, reflected in the observation that the oscillatory frequency of n and $\langle S^z \rangle$ is twice that of $\langle S^x \rangle$. The time-averaged value of $\langle S^x \rangle$ becomes nonzero at the transition from L1 to L2, which can be explained by the spontaneous breaking of the \mathbb{Z}_2 symmetry upon increasing the Dicke coupling λ [cf. Fig. 2(c)]. The transition from the SR region to the L2 region appears as a crossover in finite-time numerical data, as the damping of the oscillations of $\langle S^x \rangle$ critically slows down upon approaching the transition point from the SR side, hence the time-averaged amplitude of the oscillations in long but finite time windows smoothly grows, blurring the expected singular behavior at the phase boundary [cf. Fig. 2(b)] associated to the dynamical spontaneous symmetry breaking of the $U(1)$ symmetry. Finally, in the transition from NS to L2, the absolute value of the time average of $\langle S^x \rangle$, as well as its amplitude, build up [cf. Fig. 2(d)].

This dynamical phase diagram with competing stationary (NS, SR) and oscillatory (L1, L2, IR) phases is of great interest to spintronics, since it emerges from the interplay of incoherent spin pumping and ellipticity. We now briefly discuss some possible implications of our results. In previous studies, magnon conservation is taken to be an important ingredient in the study of coherent spin-wave lasing or magnon Bose-Einstein condensation in pumped magnetic systems [42,43]. The magnon lasing [39] features a convergence to a steady condensate density and a circular precession [42,43]. In our model, however, we explicitly induce a Dicke term that breaks $U(1)$ symmetry. For a small Dicke coupling, the spin trajectory in the L1 lasing phase becomes elliptical instead of perfectly circular. It is similarly expected that for a magnon condensate, an explicit $U(1)$ breaking induces an ellipticity in the spontaneous precession [79], accompanied by an oscillation of the condensate density. On the other hand, the emergence of the L2 phase is a much more dramatic effect, as the spin oscillation spontaneously breaks into two separate pockets, which cannot be described by any quasiequilibrium treatment. This behavior suggests that in the spintronic setup, an exotic form of lasing can be induced in the strongly $U(1)$ breaking regime lacking magnon conservation. This opens the possibility to study spin-wave lasing phenomena in a regime where both the \mathbb{Z}_2 interaction and spin pumping are sizable, and suggests richer phenomena accompanying nonequilibrium phase transitions in spintronic devices.

We also remark that during the electrical pumping, angular momentum transfers reciprocally between the magnet and metal [55]: As the itinerant electrons exert a spin torque to establish the magnon lasing, the coherent magnetic precession simultaneously pumps a spin current back into the metal [80],

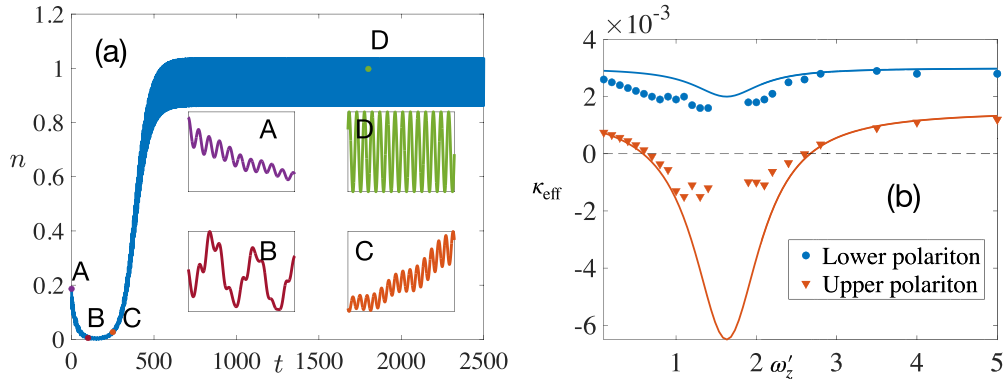


FIG. 3. (a) Dynamics of the photon number n with parameters as in Fig. 2, with the exception of ω'_z , which is chosen in resonance with the upper polariton frequency ($\omega'_z \simeq \Omega_U$). Insets show a stretched time axis. The system is prepared in the SR state and evolves with system parameters γ_\uparrow and λ inside region L1. The initial stage of dynamics is governed by the decaying lower polariton mode, while at stage C the upper polariton mode undergoes the dynamical instability triggered by the resonance with the incoherent subsystem; accordingly, the photon number starts to grow until it saturates around times $t \simeq 500$. At long times, n oscillates at the upper polariton frequency, see stage D. This is illustrative of the spin ensemble \mathcal{T} acting as a frequency-dependent gain medium. (b) The effective decay rate for the photon number $n \propto \exp(-\kappa_{\text{eff}}t)$ extracted in stage A (blue circles) and stage C (red triangles) of dynamics in (a), as a function of the frequency of the incoherent subsystem ω'_z . Close to the resonant frequency of the upper polariton, $\Omega_U = 1.63$, the effective damping $\kappa_{\text{eff}} = 2\kappa_U$ can change signs, indicating a dynamical instability, which results in the polariton lasing. Solid lines show analytical dependence according to Eq. (4).

triggering transverse spin dynamics. Therefore, suppressing the transverse spin dynamics in the metal can be detrimental to magnon lasing, as consistent with the consequence of a fast-relaxing incoherent subsystem in the Tavis-Cummings model, cf. Sec. II B. Also see below Eq. (5) for related discussion.

IV. POLARITON LASING

Observables in the L1 and L2 phases show signatures of upper (U) and lower (L) polariton modes [58], which are symmetric (U) and antisymmetric (L) linear superpositions of spin and boson fields, describing light-matter hybridization via the Dicke coupling λ . To appreciate this point, we rewrite the interaction term in Eq. (1) as $H_{\text{int}} = (\eta a + \eta' \mathcal{S}^-) \mathcal{T}^+ + \text{H.c.}$, which is suggestive that pumping the \mathcal{T} ensemble can excite a superposition of light and matter in the \mathcal{S} system. Thus, upper or lower polaritons can be excited in the system, depending on whether the two couplings have the same or opposite signs, jointly with the resonance condition, $\omega'_z \simeq \Omega_{U/L}$, where within NS the eigenfrequencies read [58]

$$\Omega_{U/L} = \sqrt{(\omega_c^2 + \omega_z^2 \pm \sqrt{(\omega_c^2 - \omega_z^2)^2 + 16\lambda^2\omega_z\omega_c})/2}. \quad (3)$$

The effective decay rates of the two polariton modes $\psi_{U,L}$ depend on the frequency of the incoherent subsystem ω'_z and, in particular, for $\eta = \eta'$, it can be analytically estimated as

$$\kappa_U = \kappa/4 - \eta^2(\gamma_\uparrow - \gamma_\downarrow)/[(\omega'_z - \Omega_U)^2 + \gamma_t^2/4]. \quad (4)$$

By tuning ω'_z close to Ω_U , it is possible to obtain a negative effective decay rate ($\kappa_U < 0$) for $\gamma_\uparrow > \gamma_\downarrow$ that induced dynamical instabilities into the system.

The boson annihilation operator a can be written as the sum of upper and lower polaritons, and thus both modes contribute to the dynamics of photon number $n = \langle a^\dagger a \rangle$. However, their effective decay rates are different, giving rise to different short- and long-time behaviors of the dynamics of

n . This can be seen explicitly by considering a quench from the stationary SR phase to the nonstationary lasing phase, as shown in Fig. 3(a). Here, we initialize the system in the SR steady state of the Dicke model with photon losses ($\lambda = 0.6$ and $\kappa = 0.06$) and let it evolve with parameters characteristic of the L1 phase ($\lambda = 0.2$, $\gamma_\uparrow = 0.9$) while keeping $\omega'_z \simeq \Omega_U$. We now discuss the multistage dynamics [as marked by A–D in Fig. 3(a)] associated with this protocol. Inside the SR phase, the difference between the amplitudes of upper and lower modes can be estimated using the Holstein-Primakoff analysis [58] as

$$\frac{|\psi_U|}{|\psi_L|} = \left| \frac{1 - 2\lambda(\omega_c + i\kappa/2)/(\omega_c^2 + \kappa^2/4)}{1 + 2\lambda(\omega_c + i\kappa/2)/(\omega_c^2 + \kappa^2/4)} \right| \approx \left| \frac{1 - 2\lambda/\omega_c}{1 + 2\lambda/\omega_c} \right|,$$

which is much smaller than 1 close to λ_c . Thus, initializing a system in the SR phase corresponds to setting it into a lower polariton mode. As we fix $\omega'_z \approx \Omega_U$ and set the rest of the parameters to be such that $\kappa_U < 0$, the upper polariton in this scenario is exponentially enhanced at the beginning of the dynamics, while the lower polariton has $\kappa_L > 0$ and thus decays. Therefore, immediately after the quench (A), the photon field has a sizable overlap with the lower polariton mode. Since in the initial SR steady state the boson is enslaved to matter [$\langle a \rangle = -2\lambda/(\omega_c - i\kappa/2)\langle \mathcal{S}^- \rangle$], the amplitude of the lower mode is larger than the amplitude of the upper one. However, as the lower mode starts to decay and the upper one is enhanced, their amplitudes become comparable (B) and we observe beating at their two frequencies. At stage (C), the photon number increases while the lower mode is largely suppressed. As a result, for long times (D), the oscillatory dynamics of the system is solely governed by Ω_U . Such circumstances cannot occur in a more conventional driven-dissipative Dicke model [75] since, in that case, both upper and lower modes would be enhanced and survive at long times.

Finally, we verify the dependence in Eq. (4) numerically by studying the relaxation of the system after quenching from the SR phase to the nonstationary lasing phase. We extract the effective decay rate of the photon mode, which is given by $n = \langle a^\dagger a \rangle \propto \exp(-\kappa_{\text{eff}} t)$, in different parametric regimes. Depending on the level splitting of the \mathcal{T} spins, ω'_z , κ_{eff} can be varied. Figure 3(b) shows the effective damping κ_{eff} of the photon mode as a function of ω'_z . The effective damping coefficients $\kappa_{U/L}$ of the lower and upper modes are extracted from the dynamics of n at short [stage (A) in Fig. 3(a)] and long [stage (C) in Fig. 3(a)] timescales, respectively. As one can see from Fig. 3(b), both damping coefficients have a minimum close to the resonance upper polariton frequency. Also, for all frequencies ω'_z , the damping of the lower mode is faster than that of the upper polariton, which is why we observe oscillations at long times with frequency Ω_U only. The upper mode is long-lived and can even be enhanced via pumping when ω'_z is close enough to the upper polariton frequency Ω_U , resulting in lasing.

If the system is pumped resonantly with the upper polariton frequency $\omega'_z \simeq \Omega_U$, the critical value of γ_\uparrow at which the lasing region occurs can be estimated as

$$\frac{\gamma_\uparrow}{\gamma_t} \geq \frac{1}{2} \left(\frac{\kappa \gamma_t}{16\eta^2} + 1 \right), \quad (5)$$

following a calculation similar to the one in Sec. II B. This also constrains the condition between pumping/relaxation rates and coherent coupling η under which non-stationary phases can be observed, i.e., the right-hand side of Eq. (5) cannot exceed 1. Otherwise, the typical relaxation time of the incoherent subsystem $\mathcal{T} \propto 1/\gamma_t$ is faster than growing time of the coherent subsystem [59,60], which means that mutual dynamics of the coherent and incoherent parts does not have time to establish itself. For the polariton mode, lasing is obtained at a pumping frequency smaller than the conventional threshold for lasing $\omega'_z \leq \Omega_U + \sqrt{4\eta^2(\gamma_\uparrow - \gamma_\downarrow)/\kappa - \gamma_t^2}/4$. Similarly, the lower polariton mode can be resonantly pumped when $\eta = -\eta'$. In this case, the effective damping for both modes have a minimum at the lower polariton frequency Ω_L .

V. CONCLUSION AND OUTLOOK

In this paper, we bridge cavity QED and spintronics communities by suggesting the model that could find the implementation in both areas. We have captured the essential overlapping ingredients with a particular focus on the symmetry properties and shown that our approach can promote discovery of new dynamical phases with nontrivial interpretation from both standpoints. A further development of our model (1) and the accessibility of different parametric regimes in different platforms can be inspiring for the study of emergent dynamical phenomena in general.

A natural next step forward would consist of studying collective spin squeezing in the lasing regime [81–83], with the perspective of entanglement manipulation in spintronics platforms. This can be addressed, for instance, by simulating numerically exact dynamics at finite N [84,85].

Recent studies have shown the usefulness of nonlocal dissipation in generating entanglement between distant qubits in both fields of quantum optics and spintronics, by investigating spins immersed in an optical cavity [14,15,86] and nitrogen-vacancy qubits in proximity to a magnetic medium [87]. For the latter, dynamical phase transitions in the magnet controlled by electrical pumping may provide an efficient tunability of nonlocal dissipation, which could be studied along the lines of this paper.

Finally, we did not include here the effect of short-range spin interactions breaking permutational symmetry. This is, in general, a challenging task since it requires a full many-body treatment of dynamics. However, we expect that, deep inside the various phases, the dynamical phenomena discussed here will still hold in analogy with the character of other nonequilibrium phases in spin systems with competing short- and all-to-all interactions [68,88,89].

Our results can be considered as a roadmap to build a generation of spintronics experiments inspired by quantum optics, with a focus on dynamical phase transitions in heterolayer structures. Scaling up our proof of concept to more concrete platforms appears to be an exciting future direction.

ACKNOWLEDGMENTS

J.M. and O.C. are indebted to P. Kirton for enlightening discussions. O.C. thanks S. Kelly and R. J. Valencia-Tortora for helpful comments on this paper. This project has been supported by the Deutsche Forschungsgemeinschaft (DFG, German Research Foundation) through the Project ID 429529648—TRR 306 (“QuCoLiMa Quantum Cooperativity of Light and Matter”), by the Dynamics and Topology Centre funded by the State of Rhineland Palatinate, and in part by the National Science Foundation under Grant No. NSF PHY-1748958 (KITP program Non-Equilibrium Universality: From Classical to Quantum and Back). J.M. and O.C. acknowledge support by the Dynamics and Topology Centre funded by the State of Rhineland Palatinate. A.L. acknowledges support by the Swiss National Science Foundation. S.Z. and Y.T. are supported by the U.S. Department of Energy, Office of Basic Energy Sciences under Grant No. DE-SC0012190. The Alexander von Humboldt Foundation is acknowledged for supporting Y.T.’s stay at Mainz, where this work was initiated. I.C. acknowledges financial support from the H2020-FETFLAG-2018-2020 project PhoQuS (No. 820392) and from the Provincia Autonoma di Trento.

APPENDIX A: STABILITY ANALYSIS

The mean-field equations of motion used to derive the phase diagram in Fig. 2(a) read

$$\begin{aligned} \frac{d\langle a \rangle}{dt} &= -i\eta \langle \mathcal{T}^- \rangle - (i\omega_c + \kappa/2) \langle a \rangle - i\lambda (\langle \mathcal{S}^+ \rangle + \langle \mathcal{S}^- \rangle) \\ \frac{d\langle \mathcal{S}^z \rangle}{dt} &= i\lambda (\langle a \rangle + \langle a^\dagger \rangle) (\langle \mathcal{S}^- \rangle - \langle \mathcal{S}^+ \rangle) \\ &\quad + i\eta' (\langle \mathcal{T}^+ \rangle \langle \mathcal{S}^- \rangle - \langle \mathcal{T}^- \rangle \langle \mathcal{S}^+ \rangle) \\ \frac{d\langle \mathcal{S}^- \rangle}{dt} &= -i\omega_z \langle \mathcal{S}^- \rangle + 2i\lambda (\langle a \rangle + \langle a^\dagger \rangle) \langle \mathcal{S}^z \rangle + 2i\eta' \langle \mathcal{T}^- \rangle \langle \mathcal{S}^z \rangle \end{aligned}$$

$$\begin{aligned} \frac{d\langle \mathcal{T}^z \rangle}{dt} &= i\eta(\langle a^\dagger \rangle \langle \mathcal{T}^- \rangle - \langle a \rangle \langle \mathcal{T}^+ \rangle) - i\eta'(\langle \mathcal{T}^+ \rangle \langle \mathcal{S}^- \rangle \\ &\quad - \langle \mathcal{T}^- \rangle \langle \mathcal{S}^+ \rangle) + \frac{\gamma_\uparrow - \gamma_\downarrow}{2} - \gamma_t \langle \mathcal{T}^z \rangle \\ \frac{d\langle \mathcal{T}^- \rangle}{dt} &= -(i\omega'_z + \gamma_t/2)\langle \mathcal{T}^- \rangle + 2i\eta\langle a \rangle \langle \mathcal{T}^z \rangle + 2i\eta'\langle \mathcal{T}^z \rangle \langle \mathcal{S}^- \rangle, \end{aligned} \quad (\text{A1})$$

where $\langle \cdot \rangle$ stands for the ensemble-averaged value of an observable. Here we neglected higher order correlations which are all suppressed as $1/N$, approximating $\langle AB \rangle \approx \langle A \rangle \langle B \rangle$. This

$$A = \begin{bmatrix} -i\omega_c - \frac{\kappa}{2} & 0 & -i\lambda & -i\lambda & -i\eta & 0 \\ 0 & i\omega_c - \frac{\kappa}{2} & i\lambda & i\lambda & 0 & i\eta \\ -i\lambda & -i\lambda & -i\omega_z & 0 & -i\eta' & 0 \\ i\lambda & i\lambda & 0 & i\omega_z & 0 & i\eta' \\ 2i\eta\langle \mathcal{T}^z \rangle & 0 & 2i\eta'\langle \mathcal{T}^z \rangle & 0 & -i\omega'_z - \frac{\gamma_t}{2} & 0 \\ 0 & -2i\eta\langle \mathcal{T}^z \rangle & 0 & -2i\eta'\langle \mathcal{T}^z \rangle & 0 & i\omega'_z - \frac{\gamma_t}{2} \end{bmatrix}. \quad (\text{A2})$$

By performing a stability analysis [75], one can distinguish the set of parameters for which the NS is stable (cf. Fig. 4). The white region with all negative eigenvalues corresponds to the stable normal phase. The purple region with one real positive eigenvalue matches the boundary of the SR phase in Fig. 2(a). The yellow region with two positive complex conjugate eigenvalues corresponds to lasing. The parameters in the orange region corresponds to the three positive eigenvalues of the matrix Eq. (A2). The boundary between the SR and NS is well approximated by the λ_c of the Dicke model [58,75]. However, this simple stability analysis does not capture the

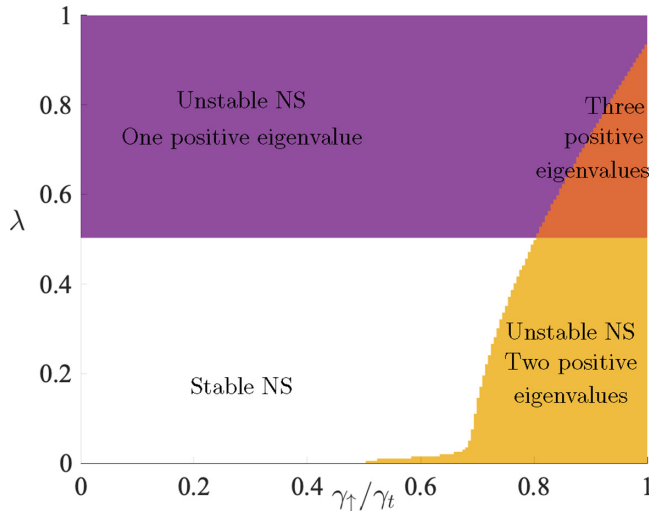


FIG. 4. Stability analysis of the normal state. The parameters are the same as in Fig. 2(a). The stable normal state is indicated in white. The purple color corresponds to one real positive eigenvalue of the matrix A and it indicates superradiance. The yellow region corresponds to two complex conjugated eigenvalues with positive real part and it corresponds to the lasing region. The orange region corresponds to the three positive eigenvalues. Here $\omega = \omega'_z$.

approximation is exact in the $N \rightarrow \infty$ limit [57]. All variables in Eqs. (A1) are intensive, since they are normalized in such a way that they are independent of the number of spins N as $N \rightarrow \infty$.

From the equation above, we study the instabilities of the NS. By perturbing with small fluctuations around the NS expectation values $\langle a \rangle = \langle a \rangle_0 + \delta a$, $\langle \mathcal{S}^- \rangle = \langle \mathcal{S}^- \rangle_0 + \delta \mathcal{S}^-$, $\langle \mathcal{T}^- \rangle = \langle \mathcal{T}^- \rangle_0 + \delta \mathcal{T}^-$, (with $\langle a \rangle_0 = \langle \mathcal{S}^- \rangle_0 = \langle \mathcal{T}^- \rangle_0 = 0$, $\langle \mathcal{S}^z \rangle = -1/2$ and $\langle \mathcal{T}^z \rangle = (\gamma_\uparrow - \gamma_\downarrow)/(2\gamma_t)$), we can find a linear system of equations for these deviations from the NS, which can be written in the form $\dot{x} = Ax$, where $x = (\delta a, \delta a^*, \delta \mathcal{S}^-, \delta \mathcal{S}^+, \delta \mathcal{T}^-, \delta \mathcal{T}^+)^T$. This matrix reads

difference between dynamical phases such as L1, L2, and IR in Fig. 2(a), which require a thorough evaluation of the far-from-equilibrium dynamics encoded in Eqs. (A1).

When we pump the system at a frequency resonant with the upper polariton frequency, $\omega'_z \approx \Omega_U$, the boundary of the lasing region can undergo drastic changes. As shown in Fig. 5, in this case the boundary between the NS and lasing phase is solely set by the critical value of pumping rate γ_\uparrow/γ_t and does not depend on λ .

APPENDIX B: DICKE AND TAVIS-CUMMINGS MODELS

In this Appendix, we examine two known limits of the model (1) and their mean-field solutions.

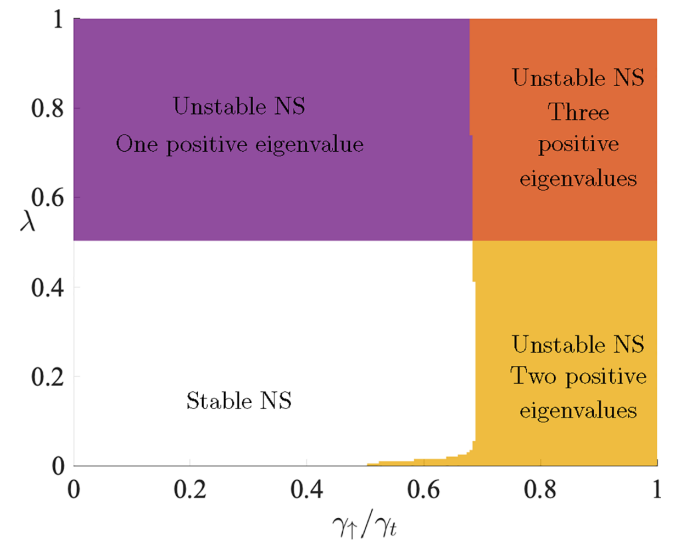


FIG. 5. Stability analysis with the resonance condition $\omega'_z = \Omega_U$. The rest of the parameters are the same as in Fig. 2(a). The vertical boundary between normal state (white) and lasing (yellow) is given by the critical pumping rate $\gamma_\uparrow^c \approx 0.7\gamma_t$ [see Eq. (5)].

In the limit of $\eta = \eta' = 0$, our model is reduced to the Dicke model with a spontaneous \mathbb{Z}_2 -breaking transition. For $\lambda < \lambda_c = \sqrt{\omega_z(\omega_c^2 + \kappa^2/4)/(4\omega_c)}$, the stationary state of Eq. (A1) is $\langle a \rangle = \langle S^{x,y} \rangle = 0$ and $\langle S^z \rangle = \pm 1/2$. For $\lambda \geq \lambda_c$, a pair of nontrivial solutions breaking the \mathbb{Z}_2 symmetry appear, such that $\langle S^z \rangle = -(1 - \lambda_c^2/\lambda^2)/2$, $\langle S^x \rangle = \pm \sqrt{1/4 - \langle S^z \rangle^2}$, $\langle a \rangle = -2\lambda \langle S^x \rangle / (\omega_c + i\kappa/2)$.

The other limit $\eta' = \lambda = 0$ corresponds to the incoherently pumped Tavis-Cummings model. For $\gamma_t \gg \eta, \eta'$, the last line of the mean-field equations of motion in Eq. (A1) shows a quick relaxation towards a steady state with $\langle \mathcal{T}^z \rangle \approx$

$(\gamma_\uparrow - \gamma_\downarrow)/(2\gamma_t) \equiv \tau_0^z$ and $\langle \mathcal{T}^\pm \rangle \approx 0$. The system is driven into a mixed state with a relative population of up and down spins controlled by the ratio γ_\uparrow/γ_t . Nontrivial solutions of the mean-field equations of motion (A1) that break dynamically the symmetry can be expressed in the form (see, for instance, Refs. [76,77])

$$\langle a \rangle \rightarrow a_0 e^{-i\Delta t}, \quad \langle \mathcal{T}^\pm \rangle \rightarrow \mathcal{T}_0^\pm e^{\pm i\Delta t}, \quad (\text{B1})$$

where Δ is a characteristic frequency to be self-consistently determined. Substituting Eqs. (B1) into Eqs. (A1), one obtains

$$\begin{aligned} \Delta &= \frac{\kappa\omega'_z + \gamma_t\omega_c}{\kappa + \gamma_t} \\ \langle \mathcal{T}^z \rangle &= \frac{\gamma_t\kappa}{2\eta^2} \left(\frac{(\omega_c - \omega'_z)^2}{(\kappa + \gamma_t)^2} + \frac{1}{4} \right) \\ \mathcal{T}_0^\pm &= \sqrt{\frac{\gamma_t\tau_0^z\kappa}{\eta^2} \left(\frac{(\omega_c - \omega'_z)^2}{(\kappa + \gamma_t)^2} + \frac{1}{4} \right) - \frac{\gamma_t^2\kappa^2}{2\eta^4} \left(\frac{(\omega_c - \omega'_z)^2}{(\kappa + \gamma_t)^2} + \frac{1}{4} \right)^2}. \end{aligned} \quad (\text{B2})$$

Further simplification is possible in the $\omega_c \approx \omega'_z \equiv \omega$ limit,

$$\begin{aligned} \Delta &= \omega \\ \langle \mathcal{T}^z \rangle &= \frac{\gamma_t\kappa}{8\eta^2} \\ \langle \mathcal{T}^\pm \rangle &= \sqrt{\frac{\gamma_t\tau_0^z\kappa}{4\eta^2} - \frac{\gamma_t^2\kappa^2}{32\eta^4}} e^{\pm i\omega t} \\ n &= \frac{\gamma_t}{\kappa} (\tau_0^z - \langle \mathcal{T}^z \rangle), \end{aligned} \quad (\text{B3})$$

from which it is clear that the lasing solution exists only if the photon loss rate is below a critical value $\kappa < \kappa_c = 4\eta^2/\gamma_t$.

APPENDIX C: GILBERT DAMPING

For the magnon condensate mode, dissipation in the form of Gilbert damping slows down the spontaneous precession of the magnetic order parameter like a viscous drag [54]. It is particularly suitable in the weak-damping scenario to describe the relaxation of the precessional motion back to the equilibrium state (in the absence of external pumping) along a spiral trajectory without losing coherence. The semiclassical Landau-Lifshitz-Gilbert equation [65,90,91] of a spin \mathbf{s} reads $d\mathbf{s}/dt = \mathbf{s} \times \mathbf{h}_{\text{eff}} - \alpha_G \mathbf{s} \times d\mathbf{s}/dt$, where \mathbf{h}_{eff} is an effective Zeeman field fixing the equilibrium spin orientation and α_G is the Gilbert damping. A small-angle spin precession can be mapped to the motion of a harmonic oscillator with creation and annihilation operators [92] a^\dagger and a , where $s_z = s - a^\dagger a \approx s$ with s being the spin length. The Landau-Lifshitz-Gilbert equation in the lowest order then becomes $(1 + i\alpha_G) d\langle a \rangle / dt = -i\omega_c \langle a \rangle$, where $\omega_c = |\mathbf{h}_{\text{eff}}|$. Such a form of the viscous drag can also be derived by coupling the bosonic mode a to an Ohmic bath and eliminating the bath degrees of freedom following a standard Caldeira-Leggett derivation [62].

For the model (1), the Gilbert damping modifies the mean-field equation of motion for the expectation value of the bosonic mode into

$$\begin{aligned} (1 + i\kappa/2) \frac{d\langle a \rangle}{dt} &= -i(\omega_c - \tilde{\Delta}) \langle a \rangle - i\eta \langle \mathcal{T}^- \rangle \\ &\quad - i\lambda (\langle S^+ \rangle + \langle S^- \rangle) + \frac{B(t)}{\sqrt{N}}. \end{aligned} \quad (\text{C1})$$

Here $\tilde{\Delta}$ is a Lamb shift and $B(t)$ is the noise term that results from the bath [62]. This term is suppressed as $1/\sqrt{N}$ for large N , therefore vanishing in the mean-field limit. The dynamical phase diagram with this type of dissipation is plotted in Fig. 6. Here we fixed $\tilde{\omega}_c = \omega_c - \tilde{\Delta} = 1$ and $\kappa = 0.04$. Qualitatively, the diagram remains the same as if we used photon losses;

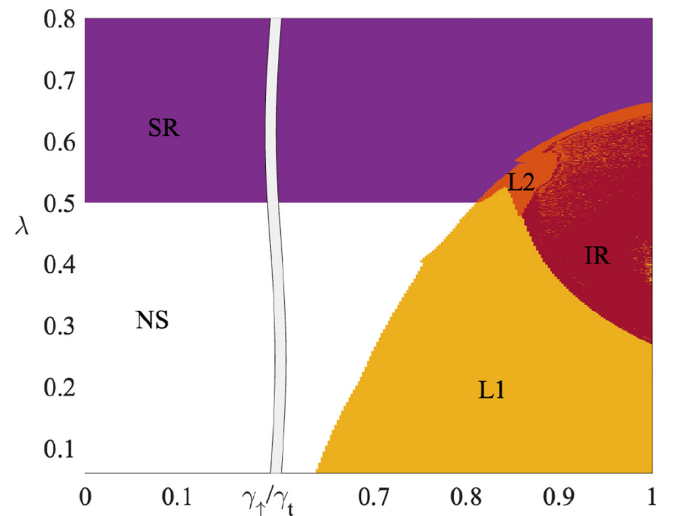


FIG. 6. Dynamical phase diagram with Gilbert damping [see Eq. (C1)]. All parameters are as in Fig. 7 and the color code follows Fig. 2(a).

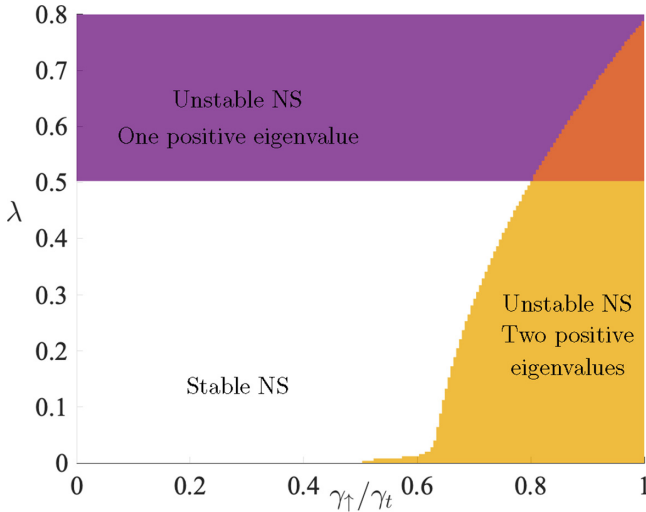


FIG. 7. Stability analysis for model with Gilbert damping. All parameters are as in Fig. 2(a), $\kappa = 0.04$, and the color code follows Fig. 4.

we still recognize five different dynamical responses as superradiance, NS, and lasing and SR persistent oscillations (L1 and L2), as well as irregular dynamics (IR), although the boundaries between phases are quantitatively modified. Results are in a good agreement with predictions obtained from the stability analysis (cf. Fig. 7).

APPENDIX D: INSTABILITIES FROM ADIABATIC ELIMINATION

We now work out analytically some dynamical properties of our system in the limit of a fast relaxing bath [93], known as adiabatic elimination of the bath in quantum optics. We choose γ_t large enough compared to η and η' to induce relaxation of the incoherent subsystem \mathcal{T} much faster than the dynamics of the coherent one \mathcal{S} . Following Refs. [94,95], we can enslave the spins of the incoherent ensembles to those of the Dicke system by setting the time derivatives of the former to zero:

$$\begin{aligned} \langle \mathcal{T}^- \rangle &\simeq \frac{2\langle \mathcal{T}^z \rangle (\omega'_z + i\gamma_t/2)}{\omega_z'^2 + \gamma_t^2/4} (\eta \langle a \rangle + \eta' \langle \mathcal{S}^- \rangle) + \dots, \\ \langle \mathcal{T}^+ \rangle &\simeq \frac{2\langle \mathcal{T}^z \rangle (\omega'_z - i\gamma_t/2)}{\omega_z'^2 + \gamma_t^2/4} (\eta \langle a^\dagger \rangle + \eta' \langle \mathcal{S}^+ \rangle) + \dots \\ \langle \mathcal{T}^z \rangle &\simeq (\gamma_\uparrow - \gamma_\downarrow)/2\gamma_t + \dots, \end{aligned} \quad (\text{D1})$$

where we neglect terms in higher orders of $1/\gamma_t$. This is equivalent to assuming that spins in the \mathcal{T} ensemble have already reached their steady state. When substituting Eq. (D1) into the equations of motion for the normalized cavity mode and for the spins of the coherent subsystem \mathcal{S} , we find

$$\begin{aligned} \langle \dot{a} \rangle &= - \left(i\omega_c + \frac{\kappa}{2} \right) \langle a \rangle - i\eta \left(\frac{2\eta \langle \mathcal{T}^z \rangle}{\omega_z' - i\gamma_t/2} \langle a \rangle \right. \\ &\quad \left. + \frac{2\eta' \langle \mathcal{T}^z \rangle}{\omega_z' - i\gamma_t/2} \langle \mathcal{S}^- \rangle \right) - i\lambda (\langle \mathcal{S}^+ \rangle + \langle \mathcal{S}^- \rangle). \end{aligned} \quad (\text{D2})$$

The dissipative dynamics of the subsystem \mathcal{S} and the photon mode can now be described with Lindblad terms with effective jump operators $L_1 = \sqrt{\gamma_\uparrow} \tau_i^+$ and $L_2 = \sqrt{\gamma_\downarrow} \tau_i^-$, given in terms of a and \mathcal{S}^- through Eqs. (D1). From Eq. (D2), we find

$$\langle \dot{a} \rangle = (-i\tilde{\omega} - \tilde{\kappa}) \langle a \rangle - i\lambda (\langle \mathcal{S}^+ \rangle + \langle \mathcal{S}^- \rangle) - \frac{2i\eta\eta' \langle \mathcal{T}^z \rangle}{\omega_z' - i\gamma_t/2} \langle \mathcal{S}^- \rangle, \quad (\text{D3})$$

where

$$\tilde{\omega} = \omega_c - \frac{2\eta^2 \omega_z' \langle \mathcal{T}^z \rangle}{\omega_z'^2 + \gamma_t^2/4}, \quad \tilde{\kappa} = \frac{\kappa}{2} - \frac{\gamma_\uparrow - \gamma_\downarrow}{2} \frac{\eta^2}{\omega_z'^2 + \gamma_t^2/4}. \quad (\text{D4})$$

According to the last formula in Eqs. (D4), when the incoherent ensemble is in the population inverted state, the photon mode becomes effectively pumped due to the weak interaction with \mathcal{T} . If this pumping overcomes the photon decay κ , the photon number starts to grow and dynamical instabilities are triggered.

The equation that effectively governs the dynamics of the coherent subsystem can be derived in the same way and reads

$$\begin{aligned} \langle \dot{\mathcal{S}}^- \rangle &= -i\omega_z \langle \mathcal{S}^- \rangle + 2i\lambda (\langle a \rangle + \langle a^\dagger \rangle) \langle \mathcal{S}^z \rangle \\ &\quad + \frac{2i\eta' (\omega_z' + i\gamma_t/2) (\gamma_\uparrow - \gamma_\downarrow) \langle \mathcal{S}^z \rangle}{\gamma_t (\omega_z'^2 + \gamma_t^2/4)} (\eta \langle a \rangle + \eta' \langle \mathcal{S}^- \rangle). \end{aligned}$$

Here the effective contribution from the dissipator has the form

$$\langle \dot{\mathcal{S}}^- \rangle \propto \frac{\eta' (\gamma_\uparrow - \gamma_\downarrow) (-\langle \mathcal{S}^z \rangle)}{\omega_z'^2 + \gamma_t^2/4} (\eta \langle a \rangle + \eta' \langle \mathcal{S}^- \rangle).$$

Therefore, for regions with $\gamma_\uparrow > \gamma_\downarrow$, spins in the system are effectively pumped by a rate proportional to the magnetization along \hat{z} , provided $\langle \mathcal{S}^z \rangle$ is negative (as it occurs in the NS or in the SR phase).

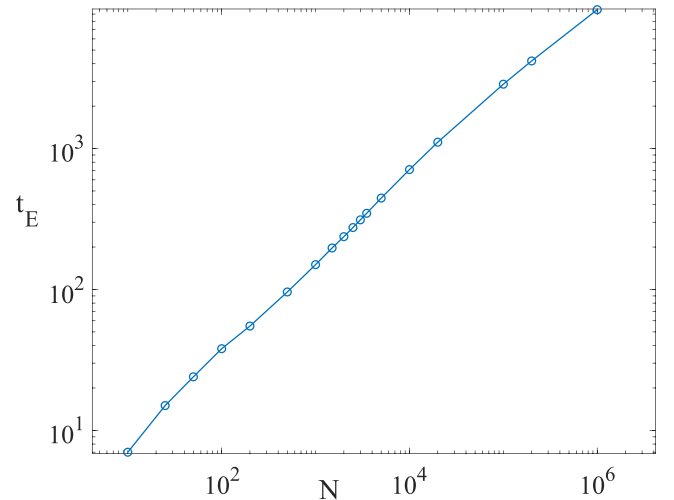


FIG. 8. Fit of the timescale $t_E \propto N^\delta$ with $\delta \simeq 0.5$ as a function of number of spins in the system, N , within the lasing region. We extract t_E as the time when the ratio between second cumulants and mean-field expectation values becomes of order ~ 0.1 .

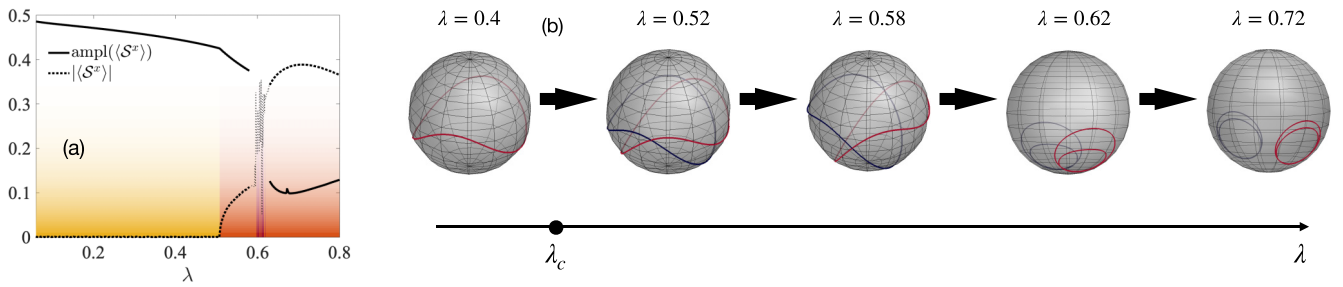


FIG. 9. (a) Amplitude of the oscillations of the $\langle S^x \rangle$ (solid line) and absolute value of the time-averaged $\langle S^x \rangle$ (dashed line) as a function of λ . We choose all parameters as in Fig. 2 and fixed $\gamma_\uparrow = 0.9\gamma_\downarrow$. The colors are the same as in Fig. 2. Yellow, orange, and red colors correspond to L1, L2, and IR phases, respectively. (b) Dynamics of the spin $\langle S \rangle$ on the Bloch sphere inside L1 and L2 regions for different values of λ . Note that inside the L2 region, depending on the initial conditions, one of two trajectories is possible with opposite time-averaged values of $\langle S^x \rangle_t = \pm s_0^x$.

Adiabatic elimination of the incoherent subsystem gives correct predictions for $\lambda = 0$. For $\lambda \neq 0$, light and matter hybridize and a separate analysis is required, see Sec. IV.

APPENDIX E: SEMICLASSICAL ANALYSIS

In models with collective, permutation-symmetric interactions, one can consider the leading effect of $1/N$ corrections beyond mean field by including second-order connected correlation functions [96,97]. In general, for finite values of N , all higher order connected correlations are relevant for dynamics; however, their effect is expected to be parametrically small in increasing powers of $1/N$ (if N is large). This is at the root of the solvability of models with all-to-all interactions mediated by a common bosonic mode, as in our system: the BBGKY hierarchy [98,99] closes when large system sizes are considered, allowing for nonperturbative solutions in the couplings governing both unitary or dissipative dynamics.

We include two-point connected correlation functions which couple to mean-field motion, neglecting third and higher order cumulants by approximating three point functions by their disconnected component

$$\langle ABC \rangle \simeq \langle AB \rangle \langle C \rangle + \langle AC \rangle \langle B \rangle + \langle BC \rangle \langle A \rangle - 2\langle A \rangle \langle B \rangle \langle C \rangle.$$

We simulate the dynamics and compare them with the mean-field solution to estimate the timescale, t_E , where cumulants

have sufficiently grown to invalidate the mean-field description. We find that inside the L1 phase, t_E scales as the square root of the number of spins (cf. Fig. 8). After t_E , one would have to take into account higher order correlations to correctly predict the dynamics. At times $t \sim O(N)$, the dynamics of correlations undergo phase diffusion [100,101].

APPENDIX F: DIFFERENCE BETWEEN L1 AND L2 REGIONS

In this section, we consider how the transition between phases L1 and L2 is captured in dynamics of observables. As we pointed out in Sec. III, inside the L1 region the dynamics have unbroken \mathbb{Z}_2 symmetry. Spins components oscillate in time; the frequency of oscillations of $\langle S^z \rangle$ is twice the frequency of oscillations of $\langle S^x \rangle$ and $\langle S^y \rangle$. These latter two observables have zero time average. By increasing λ above λ_c , the time-averaged value of $\langle S^x \rangle$ becomes finite $\langle S^x \rangle_t = \pm s_0^x$ while the amplitude of oscillations decreases. In Fig. 9(a), the amplitude of oscillations (solid line) and absolute value of the time-averaged $\langle S^x \rangle$ (dashed line) are plotted as functions of λ . In Fig. 9(b), trajectories of $\langle S \rangle$ for different values of λ are shown. Note that for $\lambda > \lambda_c$, depending on initial conditions, one of two trajectories (red or blue lines) is possible with time-averaged $\langle S^x \rangle_t = \pm s_0^x$, respectively.

[1] I. Carusotto and C. Ciuti, Quantum fluids of light, *Rev. Mod. Phys.* **85**, 299 (2013).
[2] K. C. Stitely, A. Giraldo, B. Krauskopf, and S. Parkins, Non-linear semiclassical dynamics of the unbalanced, open Dicke model, *Phys. Rev. Res.* **2**, 033131 (2020).
[3] H. Ritsch, P. Domokos, F. Brennecke, and T. Esslinger, Cold atoms in cavity-generated dynamical optical potentials, *Rev. Mod. Phys.* **85**, 553 (2013).
[4] J. Marini, M. Eckstein, M. Foster, and A.-M. Rey, Dynamical phase transitions in the collisionless pre-thermal states of isolated quantum systems: Theory and experiments, *Rep. Prog. Phys.* **85**, 116001 (2022).
[5] A. A. Houck, H. E. Türeci, and J. Koch, On-chip quantum simulation with superconducting circuits, *Nat. Phys.* **8**, 292 (2012).

[6] A. Kirilyuk, A. V. Kimel, and T. Rasing, Ultrafast optical manipulation of magnetic order, *Rev. Mod. Phys.* **82**, 2731 (2010).
[7] E. M. Kessler, G. Giedke, A. Imamoglu, S. F. Yelin, M. D. Lukin, and J. I. Cirac, Dissipative phase transition in a central spin system, *Phys. Rev. A* **86**, 012116 (2012).
[8] E. Janitz, M. K. Bhaskar, and L. Childress, Cavity quantum electrodynamics with color centers in diamond, *Optica* **7**, 1232 (2020).
[9] F. Mivehvar, F. Piazza, T. Donner, and H. Ritsch, Cavity qed with quantum gases: New paradigms in many-body physics, *Adv. Phys.* **70**, 1 (2021).
[10] R. Rosa-Medina, F. Ferri, F. Finger, N. Dogra, K. Kroeger, R. Lin, R. Chitra, T. Donner, and T. Esslinger, Observing

- Dynamical Currents in a Non-Hermitian Momentum Lattice, *Phys. Rev. Lett.* **128**, 143602 (2022).
- [11] S. P. Kelly, A. M. Rey, and J. Marino, Effect of Active Photons on Dynamical Frustration in Cavity QED, *Phys. Rev. Lett.* **126**, 133603 (2021).
- [12] M. A. Perlin, D. Barberena, M. Mamaev, B. Sundar, R. J. Lewis-Swan, and A. M. Rey, Engineering infinite-range SU(n) interactions with spin-orbit-coupled fermions in an optical lattice, *Phys. Rev. A* **105**, 023326 (2022).
- [13] R. Lin, R. Rosa-Medina, F. Ferri, F. Finger, K. Kroeger, T. Donner, T. Esslinger, and R. Chitra, Dissipation-Engineered Family of Nearly Dark States in Many-Body Cavity-Atom Systems, *Phys. Rev. Lett.* **128**, 153601 (2022).
- [14] K. Seetharam, A. Lerose, R. Fazio, and J. Marino, Correlation engineering via nonlocal dissipation, *Phys. Rev. Res.* **4**, 013089 (2022).
- [15] K. Seetharam, A. Lerose, R. Fazio, and J. Marino, Dynamical scaling of correlations generated by short- and long-range dissipation, *Phys. Rev. B* **105**, 184305 (2022).
- [16] A. Rauschenbeutel, P. Bertet, S. Osnaghi, G. Nogues, M. Brune, J.-M. Raimond, and S. Haroche, Controlled entanglement of two field modes in a cavity quantum electrodynamics experiment, *Phys. Rev. A* **64**, 050301(R) (2001).
- [17] M. J. Kastoryano, F. Reiter, and A. S. Sørensen, Dissipative Preparation of Entanglement in Optical Cavities, *Phys. Rev. Lett.* **106**, 090502 (2011).
- [18] K. Baumann, C. Guerlin, F. Brennecke, and T. Esslinger, Dicke quantum phase transition with a superfluid gas in an optical cavity, *Nature (London)* **464**, 1301 (2010).
- [19] F. Mivehvar, F. Piazza, and H. Ritsch, Disorder-Driven Density and Spin Self-Ordering of a Bose-Einstein Condensate in a Cavity, *Phys. Rev. Lett.* **119**, 063602 (2017).
- [20] N. Dogra, M. Landini, K. Kroeger, L. Hruby, T. Donner, and T. Esslinger, Dissipation-induced structural instability and chiral dynamics in a quantum gas, *Science* **366**, 1496 (2019).
- [21] F. Ferri, R. Rosa-Medina, F. Finger, N. Dogra, M. Soriente, O. Zilberberg, T. Donner, and T. Esslinger, Emerging Dissipative Phases in a Superradiant Quantum Gas with Tunable Decay, *Phys. Rev. X* **11**, 041046 (2021).
- [22] F. Finger, R. Rosa-Medina, N. Reiter, P. Christodoulou, T. Donner, and T. Esslinger, Spin- and momentum-correlated atom pairs mediated by photon exchange, [arXiv:2303.11326](https://arxiv.org/abs/2303.11326).
- [23] J. D. Wilson, S. B. Jäger, J. T. Reilly, A. Shankar, M. L. Chiofalo, and M. J. Holland, Beyond one-axis twisting: Simultaneous spin-momentum squeezing, *Phys. Rev. A* **106**, 043711 (2022).
- [24] J. J. Hauser, Magnetic proximity effect, *Phys. Rev.* **187**, 580 (1969).
- [25] E. Saitoh, M. Ueda, H. Miyajima, and G. Tatara, Conversion of spin current into charge current at room temperature: Inverse spin-Hall effect, *Appl. Phys. Lett.* **88**, 182509 (2006).
- [26] K. Uchida, J. Xiao, H. Adachi, J. Ohe, S. Takahashi, J. Ieda, T. Ota, Y. Kajiwara, H. Umezawa, H. Kawai, G. E. Bauer, S. Maekawa, and E. Saitoh, Spin Seebeck insulator, *Nat. Mater.* **9**, 894 (2010).
- [27] Y. Kajiwara, K. Harii, S. Takahashi, J. Ohe, K. Uchida, M. Mizuguchi, H. Umezawa, H. Kawai, K. Ando, K. Takanashi *et al.*, Transmission of electrical signals by spin-wave interconversion in a magnetic insulator, *Nature (London)* **464**, 262 (2010).
- [28] F. D. Czeschka, L. Dreher, M. S. Brandt, M. Weiler, M. Althammer, I.-M. Imort, G. Reiss, A. Thomas, W. Schoch, W. Limmer, H. Huebl, R. Gross, and S. T. B. Goennenwein, Scaling Behavior of the Spin Pumping Effect in Ferromagnet-Platinum Bilayers, *Phys. Rev. Lett.* **107**, 046601 (2011).
- [29] S. Y. Huang, X. Fan, D. Qu, Y. P. Chen, W. G. Wang, J. Wu, T. Y. Chen, J. Q. Xiao, and C. L. Chien, Transport Magnetic Proximity Effects in Platinum, *Phys. Rev. Lett.* **109**, 107204 (2012).
- [30] M. Althammer, S. Meyer, H. Nakayama, M. Schreier, S. Altmannshofer, M. Weiler, H. Huebl, S. Geprägs, M. Opel, R. Gross, D. Meier, C. Klewe, T. Kuschel, J.-M. Schmalhorst, G. Reiss, L. Shen, A. Gupta, Y.-T. Chen, G. E. W. Bauer, E. Saitoh *et al.*, Quantitative study of the spin Hall magnetoresistance in ferromagnetic insulator/normal metal hybrids, *Phys. Rev. B* **87**, 224401 (2013).
- [31] T. Lin, C. Tang, and J. Shi, Induced magneto-transport properties at palladium/yttrium iron garnet interface, *Appl. Phys. Lett.* **103**, 132407 (2013).
- [32] C. Hahn, G. de Loubens, O. Klein, M. Viret, V. V. Naletov, and J. Ben Youssef, Comparative measurements of inverse spin Hall effects and magnetoresistance in YIG/Pt and YIG/Ta, *Phys. Rev. B* **87**, 174417 (2013).
- [33] C. Kittel and C. Y. Fong, *Quantum Theory of Solids* (Wiley, New York, 1963), Vol. 5.
- [34] M. I. Dyakonov and V. Perel, Current-induced spin orientation of electrons in semiconductors, *Phys. Lett. A* **35**, 459 (1971).
- [35] S. O. Demokritov, V. E. Demidov, O. Dzyapko, G. A. Melkov, A. A. Serga, B. Hillebrands, and A. N. Slavin, Bose-Einstein condensation of quasi-equilibrium magnons at room temperature under pumping, *Nature (London)* **443**, 430 (2006).
- [36] V. E. Demidov, O. Dzyapko, S. O. Demokritov, G. A. Melkov, and A. N. Slavin, Observation of Spontaneous Coherence in Bose-Einstein Condensate of Magnons, *Phys. Rev. Lett.* **100**, 047205 (2008).
- [37] R. A. Duine, A. Brataas, S. A. Bender, and Y. Tserkovnyak, Spintronics and magnon Bose-Einstein condensation, in *Universal Themes of Bose-Einstein Condensation*, edited by N. P. Proukakis, D. W. Snoke, and P. B. Littlewood (Cambridge University Press, Cambridge, 2017), p. 505-524.
- [38] T. Giamarchi, C. Rüegg, and O. Tchernyshyov, Bose-Einstein condensation in magnetic insulators, *Nat. Phys.* **4**, 198 (2008).
- [39] L. Berger, Emission of spin waves by a magnetic multilayer traversed by a current, *Phys. Rev. B* **54**, 9353 (1996).
- [40] Y. M. Bunkov and G. E. Volovik, Magnon Condensation into a Q Ball in $^3\text{He-B}$, *Phys. Rev. Lett.* **98**, 265302 (2007).
- [41] Y. M. Bunkov and G. E. Volovik, Bose-Einstein condensation of magnons in superfluid ^3He , *J Low. Temp. Phys.* **150**, 135 (2008).
- [42] S. A. Bender, R. A. Duine, and Y. Tserkovnyak, Electronic Pumping of Quasiequilibrium Bose-Einstein-Condensed Magnons, *Phys. Rev. Lett.* **108**, 246601 (2012).
- [43] S. A. Bender, R. A. Duine, A. Brataas, and Y. Tserkovnyak, Dynamic phase diagram of dc-pumped magnon condensates, *Phys. Rev. B* **90**, 094409 (2014).
- [44] E. L. Fjærbu, N. Rohling, and A. Brataas, Electrically driven Bose-Einstein condensation of magnons in antiferromagnets, *Phys. Rev. B* **95**, 144408 (2017).

- [45] S. Takei, Spin transport in an electrically driven magnon gas near Bose-Einstein condensation: Hartree-Fock-Keldysh theory, *Phys. Rev. B* **100**, 134440 (2019).
- [46] T. Wimmer, M. Althammer, L. Liensberger, N. Vlietstra, S. Geprägs, M. Weiler, R. Gross, and H. Huebl, Spin Transport in a Magnetic Insulator with Zero Effective Damping, *Phys. Rev. Lett.* **123**, 257201 (2019).
- [47] C. Hurd, *The Hall Effect in Metals and Alloys* (Springer Science & Business Media, New York, NY, 2012).
- [48] J. E. Hirsch, Spin Hall Effect, *Phys. Rev. Lett.* **83**, 1834 (1999).
- [49] Y. K. Kato, R. C. Myers, A. C. Gossard, and D. D. Awschalom, Observation of the spin Hall effect in semiconductors, *Science* **306**, 1910 (2004).
- [50] V. Sih, R. Myers, Y. Kato, W. Lau, A. Gossard, and D. Awschalom, Spatial imaging of the spin Hall effect and current-induced polarization in two-dimensional electron gases, *Nat. Phys.* **1**, 31 (2005).
- [51] J. Wunderlich, B. Kaestner, J. Sinova, and T. Jungwirth, Experimental Observation of the Spin-Hall Effect in a Two-Dimensional Spin-Orbit Coupled Semiconductor System, *Phys. Rev. Lett.* **94**, 047204 (2005).
- [52] S. O. Valenzuela and M. Tinkham, Direct electronic measurement of the spin Hall effect, *Nature (London)* **442**, 176 (2006).
- [53] J. C. Slonczewski, Current-driven excitation of magnetic multilayers, *J. Magn. Magn. Mater.* **159**, L1 (1996).
- [54] D. C. Ralph and M. D. Stiles, Spin transfer torques, *J. Magn. Magn. Mater.* **320**, 1190 (2008).
- [55] Y. Tserkovnyak and S. A. Bender, Spin Hall phenomenology of magnetic dynamics, *Phys. Rev. B* **90**, 014428 (2014).
- [56] B. Flebus, S. A. Bender, Y. Tserkovnyak, and R. A. Duine, Two-Fluid Theory for Spin Superfluidity in Magnetic Insulators, *Phys. Rev. Lett.* **116**, 117201 (2016).
- [57] P. Kirton, M. M. Roses, J. Keeling, and E. G. Dalla Torre, Introduction to the Dicke model: From equilibrium to nonequilibrium, and vice versa, *Adv. Quantum Technol.* **2**, 1800043 (2019).
- [58] C. Emary and T. Brandes, Chaos and the quantum phase transition in the Dicke model, *Phys. Rev. E* **67**, 066203 (2003).
- [59] M. J. Bhaseen, J. Mayoh, B. D. Simons, and J. Keeling, Dynamics of nonequilibrium Dicke models, *Phys. Rev. A* **85**, 013817 (2012).
- [60] J. Keeling, M. J. Bhaseen, and B. D. Simons, Collective Dynamics of Bose-Einstein Condensates in Optical Cavities, *Phys. Rev. Lett.* **105**, 043001 (2010).
- [61] F. Reiter, T. L. Nguyen, J. P. Home, and S. F. Yelin, Cooperative Breakdown of the Oscillator Blockade in the Dicke Model, *Phys. Rev. Lett.* **125**, 233602 (2020).
- [62] H.-P. Breuer and F. Petruccione, *The Theory of Open Quantum Systems* (Oxford University Press on Demand, 2007).
- [63] P. Kirton and J. Keeling, Suppressing and Restoring the Dicke Superradiance Transition by Dephasing and Decay, *Phys. Rev. Lett.* **118**, 123602 (2017).
- [64] I. D. Mayergoyz, G. Bertotti, and C. Serpico, *Nonlinear Magnetization Dynamics in Nanosystems* (Elsevier, Oxford, 2009).
- [65] T. L. Gilbert, A phenomenological theory of damping in ferromagnetic materials, *IEEE Trans. Magn.* **40**, 3443 (2004).
- [66] N. Bode, S. V. Kusminskiy, R. Egger, and F. von Oppen, Scattering Theory of Current-Induced Forces in Mesoscopic Systems, *Phys. Rev. Lett.* **107**, 036804 (2011).
- [67] A. Lerose, J. Marino, B. Žunkovič, A. Gambassi, and A. Silva, Chaotic Dynamical Ferromagnetic Phase Induced by Nonequilibrium Quantum Fluctuations, *Phys. Rev. Lett.* **120**, 130603 (2018).
- [68] A. Lerose, B. Žunkovič, J. Marino, A. Gambassi, and A. Silva, Impact of nonequilibrium fluctuations on prethermal dynamical phase transitions in long-range interacting spin chains, *Phys. Rev. B* **99**, 045128 (2019).
- [69] Emanuele G. Dalla Torre, S. Diehl, M. D. Lukin, S. Sachdev, and P. Strack, Keldysh approach for nonequilibrium phase transitions in quantum optics: Beyond the Dicke model in optical cavities, *Phys. Rev. A* **87**, 023831 (2013).
- [70] J. Lang and F. Piazza, Critical relaxation with overdamped quasiparticles in open quantum systems, *Phys. Rev. A* **94**, 033628 (2016).
- [71] R. H. Dicke, Coherence in spontaneous radiation processes, *Phys. Rev.* **93**, 99 (1954).
- [72] B. M. Garraway, The Dicke model in quantum optics: Dicke model revisited, *Philos. Trans. R. Soc. A* **369**, 1137 (2011).
- [73] A. Safavi-Naini, R. J. Lewis-Swan, J. G. Bohnet, M. Gärttner, K. A. Gilmore, J. E. Jordan, J. Cohn, J. K. Freericks, A. M. Rey, and J. J. Bollinger, Verification of a Many-Ion Simulator of the Dicke Model Through Slow Quenches Across a Phase Transition, *Phys. Rev. Lett.* **121**, 040503 (2018).
- [74] M. A. Quiroz-Juárez, J. Chávez-Carlos, J. L. Aragón, J. G. Hirsch, and R. d. J. León-Montiel, Experimental realization of the classical Dicke model, *Phys. Rev. Res.* **2**, 033169 (2020).
- [75] P. Kirton and J. Keeling, Superradiant and lasing states in driven-dissipative Dicke models, *New J. Phys.* **20**, 015009 (2018).
- [76] D. Tieri, M. Xu, D. Meiser, J. Cooper, and M. Holland, Theory of the crossover from lasing to steady state superradiance, [arXiv:1702.04830](https://arxiv.org/abs/1702.04830).
- [77] W. Kopylov, M. Radonjić, T. Brandes, A. Balaž, and A. Pelster, Dissipative two-mode Tavis-Cummings model with time-delayed feedback control, *Phys. Rev. A* **92**, 063832 (2015).
- [78] Different amplitudes of oscillations of $\langle S \rangle$ spin components along the x and y directions in the presence of the Dicke-like interaction term.
- [79] A. A. Serga, C. W. Sandweg, V. I. Vasyuchka, M. B. Jungfleisch, B. Hillebrands, A. Kreisel, P. Kopietz, and M. P. Kostylev, Brillouin light scattering spectroscopy of parametrically excited dipole-exchange magnons, *Phys. Rev. B* **86**, 134403 (2012).
- [80] Y. Tserkovnyak, A. Brataas, and G. E. W. Bauer, Enhanced Gilbert Damping in Thin Ferromagnetic Films, *Phys. Rev. Lett.* **88**, 117601 (2002).
- [81] J. Ma, X. Wang, C. P. Sun, and F. Nori, Quantum spin squeezing, *Phys. Rep.* **509**, 89 (2011).
- [82] L. Pezze, A. Smerzi, M. K. Oberthaler, R. Schmied, and P. Treutlein, Quantum metrology with nonclassical states of atomic ensembles, *Rev. Mod. Phys.* **90**, 035005 (2018).
- [83] M. Koppenhöfer, P. Groszkowski, H.-K. Lau, and A. A. Clerk, Dissipative superradiant spin amplifier for enhanced quantum sensing, *PRX Quantum* **3**, 030330 (2022).
- [84] N. Shammah, S. Ahmed, N. Lambert, S. De Liberato, and F. Nori, Open quantum systems with local and collective incoherent processes: Efficient numerical simulations

- using permutational invariance, *Phys. Rev. A* **98**, 063815 (2018).
- [85] A. Lerose and S. Pappalardi, Bridging Entanglement Dynamics and Chaos in Semiclassical Systems, *Phys. Rev. A* **102**, 032404 (2020).
- [86] J. Marino, Universality Class of Ising Critical States with Long-Range Losses, *Phys. Rev. Lett.* **129**, 050603 (2022).
- [87] J. Zou, S. Zhang, and Y. Tserkovnyak, Bell-state generation for spin qubits via dissipative coupling, *Phys. Rev. B* **106**, L180406 (2022).
- [88] B. Zhu, J. Marino, N. Y. Yao, M. D. Lukin, and E. A. Demler, Dicke time crystals in driven-dissipative quantum many-body systems, *New J. Phys.* **21**, 073028 (2019).
- [89] S. P. Kelly, R. Nandkishore, and J. Marino, Exploring many-body localization in quantum systems coupled to an environment via Wegner-Wilson flows, *Nucl. Phys. B* **951**, 114886 (2020).
- [90] L. Landau and E. Lifshitz, On the theory of the dispersion of magnetic permeability in ferromagnetic bodies, in *Perspectives in Theoretical Physics* (Pergamon, Amsterdam, 1992), pp. 51–65.
- [91] T. L. Gilbert, A lagrangian formulation of the gyromagnetic equation of the magnetization field, *Phys. Rev.* **100**, 1243 (1955).
- [92] T. Holstein and H. Primakoff, Field dependence of the intrinsic domain magnetization of a ferromagnet, *Phys. Rev.* **58**, 1098 (1940).
- [93] G. S. Agarwal, R. R. Puri, and R. P. Singh, Atomic Schrödinger cat states, *Phys. Rev. A* **56**, 2249 (1997).
- [94] M. Xu, Theory of steady-state superradiance, Ph.D. thesis, University of Colorado at Boulder, 2016.
- [95] M. A. Norcia, R. J. Lewis-Swan, J. R. Cline, B. Zhu, A. M. Rey, and J. K. Thompson, Cavity-mediated collective spin-exchange interactions in a strontium superradiant laser, *Science* **361**, 259 (2018).
- [96] H. Haken, Cooperative phenomena in systems far from thermal equilibrium and in nonphysical systems, *Rev. Mod. Phys.* **47**, 67 (1975).
- [97] H. Haken, The semiclassical approach and its applications, in *Laser Theory* (Springer, Berlin, Heidelberg, 1984), pp. 173–248.
- [98] J. W. Negele and H. Orland, *Quantum Many-Particle Systems* (CRC Press, Boca Raton, 2018).
- [99] K. Huang, *Introduction to Statistical Physics* (Chapman and Hall/CRC, Boca Raton, FL, 2009).
- [100] M. Lewenstein and L. You, Quantum Phase Diffusion of a Bose-Einstein Condensate, *Phys. Rev. Lett.* **77**, 3489 (1996).
- [101] I. Amelio and I. Carusotto, Theory of the Coherence of Topological Lasers, *Phys. Rev. X* **10**, 041060 (2020).